A study of the spectral evolution during dipping in XB 1323-619 with Rossi-XTE and BeppoSAX

A&A 380, 494–503 (2001)
DOI: 10.1051/0004-6361:20011363

Astronomy & Astrophysics

A study of the spectral evolution during dipping in XB 1323–619 with Rossi-XTE and BeppoSAX

R. Barnard[1], M. Bałucińska-Church[1,2], A. P. Smale[3], and M. J. Church[1,2]

[1] School of Physics and Astronomy, University of Birmingham, Birmingham B15 2TT, UK
e-mail: robb@star.sr.bham.ac.uk; mbc@star.sr.bham.ac.uk
[2] Institute of Astronomy, Jagiellonian University, ul. Orla 171, 30-244 Cracow, Poland
[3] Laboratory for High Energy Astrophysics, Code 662, NASA/Goddard Space Flight Center, Greenbelt, MD 20771, USA
e-mail: alan@osiris.gsfc.nasa.gov

Received 18 May 2001 / Accepted 23 September 2001

Abstract. We report results from analysis of the observations of the dipping low mass X-ray binary XB 1323−619 made with *BeppoSAX* and *Rossi-XTE*. The dust-scattered halo contributes significantly in this source, and the observation made with *BeppoSAX* on 1997 August was used to provide MECS radial intensity profiles at several energies. From these, the halo fractions were obtained and thus an optical depth to dust scattering of 1.8 ± 0.4 derived. In the *Rossi-XTE* observation of April 25–28, 1997, seven X-rays dips were observed together with 7 bursts repeating approximately periodically. Non-dip and dip PCA spectra can be well-described by assuming the emission consists of point-like blackbody emission identified with the neutron star, plus Comptonized emission from an extended ADC. The blackbody temperature is 1.79 ± 0.21 keV and the cut-off power law photon index 1.61 ± 0.04. Spectral evolution in dipping is well described by progressive covering of the extended Comptonizing region by absorber plus more rapid removal of the point-like blackbody. The effects of dust scattering and of the X-ray pulsar 1SAX J1324.4–6200 also in the field of view are included in the fitting. We detect an iron line at ∼6.4 keV and its probable origin in the ADC is discussed.

Key words. X-rays: stars – stars: individual: XB 1323−619 – stars: neutron – binaries: close – accretion: accretion disks – ISM: dust, extinction

1. Introduction

XB 1323−619 is a member of the dipping class of Low Mass X-ray Binaries (LMXB) that exhibit irregular reductions, or dips, in X-ray intensity at the orbital period. It is generally accepted that these are caused by absorption in the bulge in the outer accretion disk where the flow from the companion star meets the disk (White & Swank 1982). XB 1323–619 is faint (∼3 mCrab), has a period of 2.94 hr and is remarkable as one of the small group of sources in which quasi-periodic bursting is observed. Investigation of spectral evolution during dipping reveals not only the structure and properties of the outer accretion disk, but also the nature and geometry of the emission regions, since the requirement to fit non-dip and several dip spectra strongly constrains emission models. In the dipping LMXB, the spectral changes during dipping cannot be described by absorption of one-component emission but require two emission components: point-like blackbody emission identified with the surface of the neutron star plus Comptonized emission from an extended Accretion Disk Corona (ADC) (e.g. Church et al. 1997). During dipping, the Comptonized emission is removed gradually as the extended absorber progressively overlaps the ADC to increasing extents, whereas the blackbody emission is rapidly removed as the absorber overlaps the point source. This model has been able to explain spectral evolution during dipping in the dipping LMXB (Church et al. 1997, 1998a,b; Bałucińska-Church et al. 1999, 2000). The other major type of model applied to the dipping sources comprises thermal emission from the accretion disk plus a Comptonized component (Mitsuda et al. 1989; Yoshida et al. 1995). Our two-component model has also been applied in a survey of the other classes of LMXB, i.e. the Z-track and Atoll sources, using *ASCA* and provided good fits to all sources in the survey spanning a luminosity

Send offprint requests to: M. J. Church,
e-mail: mjc@star.sr.bham.ac.uk

range 3×10^{36} erg s^{-1} to 5×10^{38} erg s^{-1} (Church & Bałucińska-Church 2001). This survey showed that a blackbody component was present in all sources; moreover, this was unlikely to originate in the accretion disk as the required values of inner radius were substantially less than the neutron star radius in many cases. However, assuming the emission was from an equatorial belt on the neutron star revealed an agreement between the half-height of this region, and the half-height of the inner, radiatively-supported disk (Church 2001), suggesting possible mechanisms by which the emitting area is determined (Church et al. 2001). These results provide further strong evidence that the blackbody emission in LMXB originates on the neutron star.

In the case of the dipping LMXB, the size of the extended Comptonizing ADC can be measured via dip ingress times. Application of this technique to several dipping sources (Church 2001) has revealed that the ADC is very extended, with radius typically 50 000 km or 15% of the accretion disk radius. Moreover, the ADC is *thin* having small height-to-radius ratio (Smale et al. 2001) since the absorber will not extend to the very large vertical distance required to cover a spherical region of vertical height 50 000 km. The very extended, thin nature of the ADC has several important consequences. Firstly, these measurements show that models in which Comptonization takes place in a central region, e.g. a small spherical region close to the neutron star must be incorrect. Secondly, the ADC covers all of the X-ray emitting disk. This together with the high optical depths to electron scattering of the ADC (Church 2001) means that all thermal emission from the disk will be Comptonized and no disk blackbody emission will be able to reach an observer. Thus blackbody emission from LMXB will originate on the neutron star, not on the disk. Finally, as the disk out to a radius of typically 50 000 km acts a source of Comptonization seed photons, the net spectrum of this part of the disk is easily shown to be very soft with kT between 0.001 and 0.1 keV for typical luminosities. Thus a recent tendency to use the COMPTT model for Comptonization with $kT \sim 1$ keV for the seed photons (e.g. Guainazzi et al. 1998) is inconsistent with the measurements of ADC radius above, and more important, is inconsistent with the assumption in this model that the Wien approximation is valid, e.g. in the range 1–10 keV, and so will lead to errors in spectral fitting results.

XB 1323−619 itself was first detected by *Uhuru* (Forman et al. 1978) and *Ariel V* (Warwick et al. 1981) and dipping and bursting discovered using *Exosat* (van der Klis et al. 1985; Parmar et al. 1989). Dip spectra revealed a component that was not absorbed in dipping, and spectral evolution was modelled by dividing the non-dip spectral form into two components, one of which was absorbed, the other unabsorbed but having decreasing normalization in dipping. This "absorbed + unabsorbed" approach was applied to several similar sources (Parmar et al. 1986; Courvoisier et al. 1986; Smale et al. 1992), however, the changing normalization was difficult to justify physically. The "progressive covering" model in which the absorber progressively overlaps an extended ADC is able to explain the unabsorbed component simply as the uncovered emission, in all such sources (e.g. Church et al. 1997; Smale et al. 2001). The point-like blackbody component is rapidly covered. During the *Exosat* observation, bursts repeated every 5.30–5.43 hr, approximately every second orbit.

A detailed study of the source was made with a 120-ks *BeppoSAX* observation (Bałucińska-Church et al. 1999) during which 12 intensity dips and 10 type I X-ray bursts took place. From the dipping, an orbital period of 2.938 ± 0.020 hr was derived. Bursting repeated regularly as seen in *Exosat*, but with a timescale of 2.40–2.57 hr, i.e. smaller than the orbital period, so that bursts marched through the dips leading to several occurrences of bursts during dips. It was demonstrated that the spectra of bursts in dips were consistent with a reduction in intensity in a totally ionized absorber, resulting from the ionization of all parts of the accretion disk by the bursts (Bałucińska-Church et al. 1999). The *BeppoSAX* broadband non-dip spectrum in the range 1–150 keV was fitted simultaneously with 3 MECS dip spectra, and the best fit was obtained using the point-source blackbody plus an extended Comptonization model referred to above. The Comptonization cut-off energy $E_{\rm CO}$ was found to be 44^{+5}_{-4} keV, indicating a relatively high mean electron temperature in the ADC of at least 15 keV. Dipping was well-described by combining this emission model with the progressive covering description of absorption. Quasi periodic oscillations have been detected in the quiescent, dipping and bursting emission (Jonker et al. 1999) using the *Rossi-XTE* observation made by the present authors.

We present here results of a study of dust scattering in XB 1323−619 made with *BeppoSAX*, and a study of dipping made with *Rossi-XTE*. The radial distribution of intensity in the *BepppoSAX* MECS instrument is used to provide the dust-scattering cross section in several energy bands, and from this the optical depth to dust scattering at 1 keV is derived. The relatively high Galactic column density ($\sim 4 \times 10^{22}$ atom cm^{-2}, Bałucińska-Church et al. 1999) means that dust scattering will affect the observed intensity of the source, by scattering both out of, and into the beam, and by introducing a time delay due to the scattering process. This delay results in non-dip photons reaching the observer during a dip, adding a contribution to the intensity in dipping. In the *Rossi-XTE* observation of XB 1323−619 all of the halo is collected as the PCA is non-imaging with a field-of-view of 1° and it is not possible to exclude the halo by selection from the central image as in the MECS.

In the present work, we have made a detailed study of spectral evolution in dipping, for the first time including the effects of dust scattering and utilizing the much higher sensitivity of the *Rossi-XTE* PCA to improve on the spectral fitting study made with *BeppoSAX* (Bałucińska-Church et al. 1999). The effects of the X-ray pulsar 1SAX 1324.4–6200 included in the field-of-view of

the source are added to the modelling. We also detect an iron line at ∼6.4 keV in this source.

2. Observations

2.1. *Rossi-XTE*

XB 1323–619 was observed with *Rossi-XTE* (Bradt et al. 1993) from 1997, April 25 22:02:56 to April 28 03:54:40, the observation spanning 200 ks. Results presented here were obtained using the Proportional Counter Array (PCA) instrument operated in Standard 2 mode with 16 s time resolution. The PCA consists of 5 non-imaging, coaligned Xe multiwire proportional counter units (PCUs) with a $1^\circ \times 1^\circ$ field of view and a total collecting area of $\sim$6500 cm^{-2} (Jahoda et al. 1996). All 5 PCUs were operating throughout 95% of this observation, and for optimum count statistics we use only this data in spectral analysis, also using only the top detector layers to minimise detector background. The data were screened to have elevation above the Earth's limb $>10^\circ$, and angular deviation of the pointing axis of the telescope from the source $<0.02^\circ$. PCA background subtraction was carried out using the latest versions of the appropriate background models for faint sources: the "faint17/faint240" models generated by the *Rossi-XTE* PCA team. Source and background spectra were compared, and data rejected above energies at which these become equal. Tests showed that in this faint source, spectral fitting results were not better constrained by use of HEXTE data. Light curves and spectra were deadtime corrected using the *Rossi-XTE* standard analysis software *Ftools 5.0.1*. Systematic errors of 1% were added to the spectra. The field of view of the PCA contained the 170 s period X-ray pulsar 1SAX J1324.4–6200 which was discovered serendipitously during the *BeppoSAX* observation of XB 1323–619 (Angelini et al. 1998). It is located 17′ from the LMXB, and although weak (1–10 keV luminosity $\sim 1.1 \times 10^{34}$ erg s^{-1}) for its lower limit distance of 3.4 kpc, makes a non-zero contribution to the spectrum of XB 1323–619, especially in deep dipping when the count rate of the LMXB is minimum. Included in the spectral fitting discussed below is a term for the pulsar using the best-fit to its *BeppoSAX* spectrum, with the normalization reduced by the factor 0.725 appropriate to the offset position of the X-ray pulsar in the PCA.

2.2. *BeppoSAX*

Data from the Medium-Energy Concentrator Spectrometer (MECS; 1.3–10 keV; Boella et al. 1997) on-board *BeppoSAX* are presented. The MECS consists of three grazing incidence telescopes with imaging gas scintillation proportional counters in their focal planes; however one of these had failed prior to the observation of XB 1323–619. The MECS is well-suited to the measurement of radial intensity profiles of a source having an excess over the point spread function due to dust scattering. The high energy (HPGSPC and PDS) instruments are not useful since the scattering takes place at low energies and the instruments are non-imaging. XB 1323–619 was observed using *BeppoSAX* between 1997 August 22 17:06 and August 24 02:02 UTC (Bałucińska-Church et al. 1999). Data were selected having elevation above the Earth's limb of $>4^\circ$ and were extracted using all of the image. The exposure in the MECS was 70 ks. Background subtraction was performed using standard files, but is not critical for this relatively bright source.

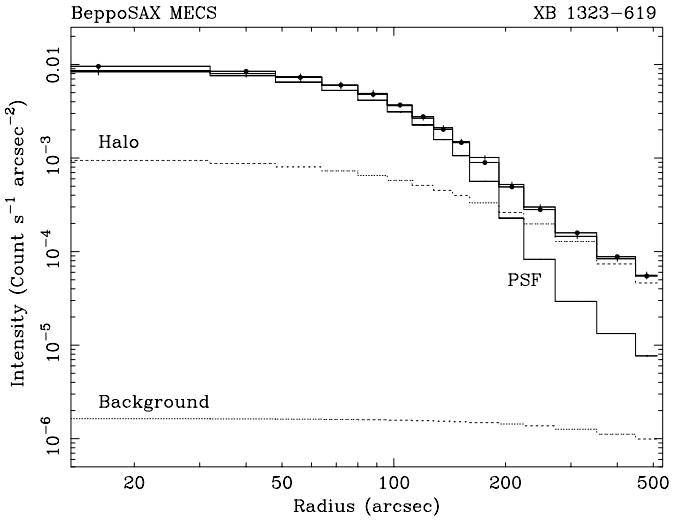

Fig. 1. Radial distribution of intensity of XB 1323−619 in the MECS in the band 1.7–2.5 keV, together with the best-fit model consisting of halo, the point-spread function and the background.

3. Results

3.1. The dust-scattering halo

The MECS instrument allows accurate determination of the radial dependence of intensity, and from measurements at several energies, the dust-scattering cross section at 1 keV can be derived. The technique was based on that used by Predehl & Schmitt (1995) in their investigation of dust scattering in 25 Galactic sources using the *Rosat* PSPC. The application of this technique to the *BeppoSAX* MECS was developed and extensively tested in the case of X 1624–490 (Bałucińska-Church et al. 2000). We apply the same technique here. The halo fraction f_h is defined via

$$f_\mathrm{h} = \frac{I_\mathrm{h}}{I_\mathrm{x} + I_\mathrm{h}}$$

where I_x is the observed source intensity and I_h the observed halo intensity. In the case of XB 1323−619 we find excesses in the radial distribution above the point spread function (PSF) for radii greater than $\sim 100''$ revealing the halo. The radial profile was extracted using

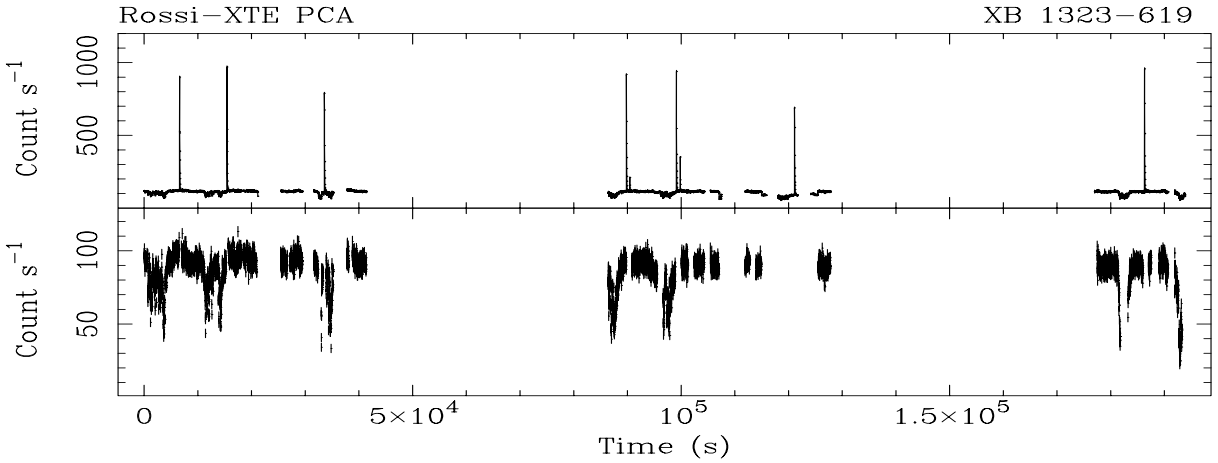

Fig. 2. Light curves of the 1997 *Rossi-XTE* observation of XB 1323–619 with 16 s binning in the band 2.0–20 keV. The scales are chosen to show bursting clearly in the upper panel, and dipping clearly in the lower panel. In both panels data were subjected to the standard screening (Sect. 2.1); in addition, in the lower panel, data were selected as for spectral analysis requiring all 5 PCUs to be operative; in the upper panel data are also included at ∼120 ks when 1 PCU was switched off since this section of data contained one of the bursts.

XIMAGE, radial bins were grouped to give a minimum of 20 counts per bin and systematic errors of 10% were added between 10–100″ where the PSF is uncertain by about this amount, and 2% between 100–500″. The radial profile was fitted between 0 and 500″, including contributions for the source convolved with the PSF, the halo, and also the background which was allowed to be a free parameter (as done by Predehl & Schmitt). The halo was calculated on the basis of Rayleigh-Gans scattering theory (Predehl & Klose 1996), although the halo fractions derived are not strongly dependent on the model used (Predehl & Klose 1996; Mathis & Lee 1991). The point spread function of Boella et al. (1997) was used. For full details of the technique, see Bałucińska-Church et al. (2000). Fits were made in several energy bands: 1.7–2.5, 2.5–3.5, 3.5–4.5, 4.5–5.5 and 5.5–6.5 keV, for which values of $f_{\rm h}$ of 0.30 ± 0.03, 0.18 ± 0.02, $0.14^{+0.01}_{-0.02}$, 0.12 ± 0.05 and $0.07^{+0.05}_{-0.06}$, respectively were found.

The reduction in source intensity due to scattering out of the beam is given by $I_{\rm x} = I_0\,{\rm e}^{-\tau}$, where τ is the optical depth to dust scattering, from which it follows that the halo fraction and τ are related by $f_{\rm h} = 1 - {\rm e}^{-\tau}$ provided the intensity scattered out of the beam is balanced by that scattered into the beam (Martin 1970). It is known that the dust-scattering cross section varies approximately as E^{-2} as expected theoretically (Mauche & Gorenstein 1986) and so τ will also vary as E^{-2}, so that

$$f_{\rm h} = 1 - {\rm e}^{-\tau_1 E^{-2}}$$

where τ_1 is the value at 1 keV. Thus from the halo fractions at several energies, we derived a value of the optical depth at 1 keV of $\tau = 1.8 \pm 0.4$. This assumed a E^{-2} dependence which appeared to fit the limited number of points adequately.

This value may be compared with the results of Predehl & Schmitt (1995) who plot τ at 1 keV against $N_{\rm H}$ for the sources in their survey and derive a relation: $\tau = 0.5\,N_{\rm H}\,[10^{22}] - 0.083$. From the best-fit value of column density from analysis of the *BeppoSAX* observation (Bałucińska-Church 1999), of $3.88 \pm 0.16 \times 10^{22}$ atom cm^{-2} we derive $\tau = 1.86$, in good agreement with the measured value. These results will be used in fitting the non-dip and dip *Rossi-XTE* data, and for determining the extent of the halo contribution to the *Rossi-XTE* 2.0–20 keV light curve (Fig. 2).

3.2. The Rossi-XTE X-ray lightcurve

Figure 2 shows the 2.0–20 keV light curve of XB 1323−619 with 16 s binning. The scales are chosen to show dipping clearly in the lower panel, and bursting clearly in the upper panel. Parts of 7 dips can be seen, and 7 X-ray bursts, two of which are double. In the lower panel, data were selected as for spectral analysis to have all 5 PCUs operative plus other screening as described in Sect. 2.1; however, there is a small part of the observation at ∼120 ks when one PCU was not operative. In the upper panel these data are included which contain one of the bursts, for which the available count rate is consequently reduced by 20%. This additional burst was included in analysis of the burst repetition rate. The bursts were found to repeat on a timescale of 2.45–2.59 hr, and the data gaps during which other bursts most probably occurred are also consistent with this recurrence timescale. In the previous *BeppoSAX* observation of 1997, August 22, the recurrence timescale of bursting was found to be 2.40–2.57 hr (Bałucińska-Church et al. 1999). This was significantly reduced compared with the timescales in the *Exosat* observation (1985, February 13) of 5.30–5.43 hr (Parmar et al. 1989) and in *ASCA* (1994, August 04) of 3.05 hr (Bałucińska-Church et al. 1999). The present observation was made on 1997, April 25, 5 months before the *BeppoSAX* observation. If we

assume, for example, that the rate of change was constant between the *Exosat* and *BeppoSAX* observations, the change per year is 0.23 hr, and the expected difference between the *BeppoSAX* and *RXTE* values would be only 0.1 hr. Further observations will reveal whether the recurrence timescale continues to decrease, or shows any dependence on luminosity (see discussion in Bałucińska-Church et al. 1999).

In the dipping, considerable variability can be seen; some dips are deep and narrow while others are broad and shallower. The depth of the dipping is ∼60%. A trend of decreasing (non-dip) intensity by ∼5% can be seen over the complete observation, and for this reason only the first 40 ks were included in spectral analysis. In Fig. 3, light curves in two energy bands 2–4 keV and 4–20 keV are shown folded on the orbital period of 2.938 hr (Bałucińska-Church et al. 1999), together with the hardness ratio formed from these. This clearly demonstrates the spectral hardening in dipping, the strong variability in dipping in this source, and that the envelope of dipping persists for a large fraction (40%) of the orbital cycle.

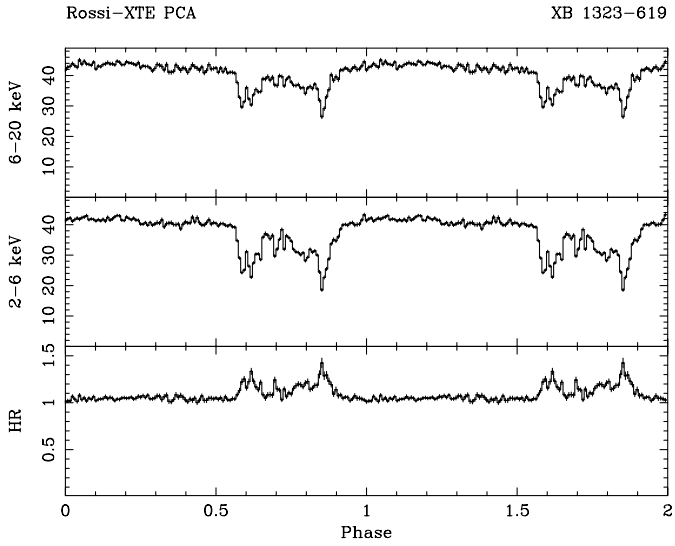

Fig. 3. Light curves in two energy bands folded on the orbital period of 2.938 hr. The lower curve shows the hardness ratio formed by dividing the light curves in the bands 4–20 keV and 2–4 keV.

To demonstrate the very strong variability in dipping, we show in Fig. 4 an expanded view of the 2.0–20 keV light curve at ∼30 ks from the start of the observations. In particular, it can be seen that each dip consists of at least 5 individual absorption events corresponding to individual blobs of absorber; in addition, most of these events show further structure. This was found to affect the results of spectral fitting in the case that dip spectra were selected by making intensity slices. Clearly, blobbiness will result in mixing data with different column densities, which will be equivalent to mixing data at different intensity levels during dipping. It is known that mixing intensity levels, e.g. by having intensity bands too wide, causes problems in spectral fitting (e.g. Church et al. 1998b). The point-source blackbody emission component contained in the best-fit model will in this case be a mixture of data in which the point-source is covered by a blob and data in which it is not covered. The result will be seen as unexpectedly low column densities for this component. Because of this, data were also selected from a single dip labelled *A* in Fig. 4 which appears to have little sub-structure. These spectra demonstrate blackbody column densities substantially higher than for the extended Comptonized emission as expected (see Sect. 3.3).

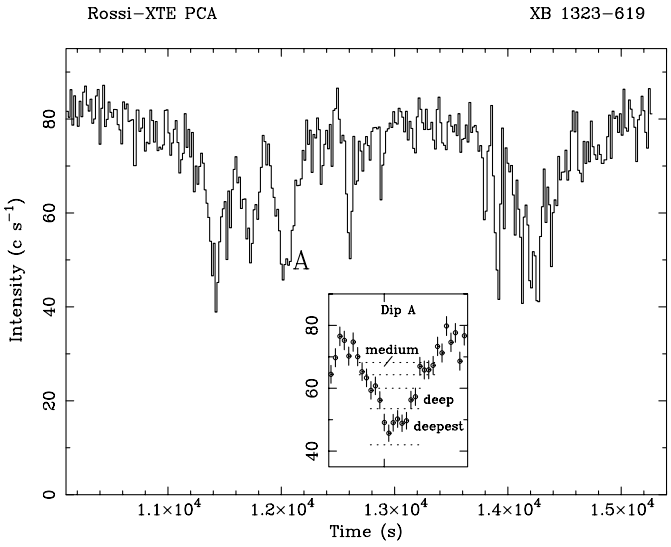

Fig. 4. Expanded light curve in the band 2.0–20 keV demonstrating the strong variability during dipping and the blobby nature of the absorber. The dip *A* is used (below) in the selection of dip spectra; the inset shows the intensity bands used for the non-dip and 3 dip spectra.

3.3. Spectral evolution during dipping

Two sets of spectra were used for spectral analysis. Firstly, data were selected from the first 40 ks of the observation in intensity bands; secondly, intensity selection was made using only the data from the individual dip *A* in Fig. 4. In the first case, data from all 5 PCUs were selected corresponding to non-dip emission and four levels of dipping chosen using bands 85–87 c s^{-1} for non-dip, 60–65, 50–55, 40–45 c s^{-1} for intermediate dipping and 35–40 c s^{-1} for deep dipping. These intensity bands were made relatively narrow to avoid as much as possible mixing data from different intensities in each spectrum. Care was also taken to exclude all traces of bursting in selecting non-dip data. An intensity band close to non-dip was avoided as experience has shown that model parameters are not well-determined in very shallow dipping. These spectra were used to eliminate various spectral models. A second set of spectra were produced from the single sub-dip *A*, consisting of a non-dip plus 3 dip levels. These spectra were used for final

fitting, allowing comparison of results with results for the first set of spectra in which dip data containing a high degree of variability in dipping are superimposed.

Using data from the first 40 ks of the observation, simple models were tested by fitting the non-dip spectrum, including absorbed bremmstrahlung (AB∗BR), absorbed blackbody (AB∗BB), absorbed power law (AB∗PL) and cut-off power law (AB∗CPL). The one-component thermal models can be rejected straight away, the blackbody model giving χ^2/d.o.f. = 2590/53, and the bremsstrahlung model giving 143/55. It is clear that the non-dip spectrum by its approximately power law nature is dominated by Comptonization, and we consider these models no further. Next, simultaneous fitting of all 5 spectra was carried out in the band 2.5–25 keV where the source is significantly detected above the background, this constraining possible models much more strongly that fitting a single non-dip spectrum. In each case, the emission parameters specifying the model were chained to be equal for all spectra fitted, and only the absorption terms were allowed to vary. Our best-fit model (below) requires inclusion of an Fe line, of the pulsar contribution and the effects of the halo. Consequently, we performed a second stage of testing the other models in which the additional 3 terms were also included. Results are shown in Table 1 for the AB∗PL, AB∗CPL models, and for progressive covering of Comptonized emission model: PCF∗CPL. Finally, the two-component model AB∗BB + PCF∗CPL was tried, consisting of blackbody emission identified with the neutron star plus Comptonized emission from an extended ADC. The point-like blackbody is covered rapidly whereas the extended Comptonized emission is progressively covered as the absorber moves across the source. Comptonized emission was modelled by a cut-off power law as the energy range of the PCA extends into the region where Comptonization down-curving is expected, and a power law approximation would be invalid. However, the cut-off energy $E_{\rm CO}$ is not very well constrained in the PCA, and so this was fixed at the value obtained from the broad band of *BeppoSAX* of 44 keV (Bałucińska-Church et al. 1999). It can be seen that there is a significant improvement in fit by adding the blackbody to the progressively covered Comptonized component (third model). An F-test showed that the presence of the additional term is significant at ≫99.9% confidence level. A similar result was obtained from the *BeppoSAX* observation of XB 1323−619 (Bałucińska-Church et al. 1999), so that the blackbody, although weak, is shown to be present.

Table 1. Results of fitting simultaneously the 5 PCA non-dip and dip spectra selected from the first 40 ks of data with various one-component and two-component models. In each case the model also has an Fe line, a pulsar contribution and halo terms as required in the case of the best-fit BB+CPL model (see text). $N_{\rm H}$ is in units of 10^{22} atom cm^{-2}.

Model	$N_{\rm H}^{\rm Gal}$	kT keV	Γ	$E_{\rm CO}$ keV	χ^2/d.o.f.
PL	4.7 ± 0.1	...	1.94 ± 0.02	...	1086/266
CPL	4.5 ± 0.1	...	1.89 ± 0.01	>180	1133/265
PCF∗CPL	6.1 ± 0.3	...	1.91 ± 0.02	>117	336/261
BB+PCF∗CPL	2.7 ± 0.6	1.36 ± 0.06	1.23 ± 0.07	44	259/256

Use of the two-component model without a line revealed residuals at about the position of an iron line, too strong to be due to remaining uncertainty in the instrument response function, and so a Gaussian line was added to the model. The non-dip spectrum provided a line energy of 6.43 ± 0.21 keV; the line width σ was fixed at an appropriate value (0.4 keV) as is usually required to stabilise the fitting of a relatively broad line. This width was found to be approximately correct, but free fitting of σ was not possible as the value tends to increase to several keV as part of the continuum becomes incorrectly modelled by the line. The equivalent width of the line was found to be 110 ± 55 eV. An upper limit $EW = 344$ eV was found for a broad line using the *Exosat* GSPC (Gottwald et al. 1995). The rather short exposure of 16 ks with *ASCA* also allowed only an upper limit EW to be obtained, equal to 26 eV although this was for an assumed energy of 6.7 keV (Asai et al. 2000). In dipping, the line was modelled firstly as a component subject only to Galactic absorption, i.e. without additional absorption in dipping, but with free normalization. The results of this were not conclusive; although there was a decrease of line intensity in shallow dipping, the line appeared at about its non-dip strength in the deepest dip spectrum. This is further discussed below.

The two-component model used at this stage has the form:

$$\mathrm{AG}\,\mathrm{e}^{-\tau}\big[\,\mathrm{AB}{*}\mathrm{BB}{+}\mathrm{PCF}{*}\mathrm{CPL}{+}\mathrm{GAU}\big] + \mathrm{AG}'{*}\mathrm{PL} + \mathrm{AG}\,\big[1-\mathrm{e}^{\tau}\big]\,\big[\mathrm{BB}{+}\mathrm{CPL}{+}\mathrm{GAU}\big].$$

Dust scattering is included by the factor $\mathrm{e}^{-\tau}$ which represents scattering out of the beam, and $(1 - \mathrm{e}^{-\tau})$ for scattering into the beam. Non-standard spectral components were produced for these for use within the *XSPEC* package. For the non-dip spectrum, the loss by scattering is balanced by the intensity scattered into the beam. In dip spectra, the gain depends on the non-dip intensity while the loss depends on the dip intensity so that the gain exceeds the loss. The X-ray pulsar is included as a constant power law term which does not vary during dipping having its own Galactic column density AG′ of 7.8×10^{22} atom cm^{-2} and power law index 1.0 (Angelini et al. 1998). Results are given in Table 2. In this fitting the line was included as a constant component; allowing the normalization to vary did not substantially improve the quality of the fits.

It can be seen that the covering fraction f increases in a systematic way as dipping gets deeper, with the column density $N_{\rm H}^{\rm CPL}$ increasing as the overlap between extended absorber and the extended ADC source becomes larger. However, the blackbody column density $N_{\rm H}^{\rm BB}$ is smaller at each level than the column of the extended emission component. In the present observation, the source is weak

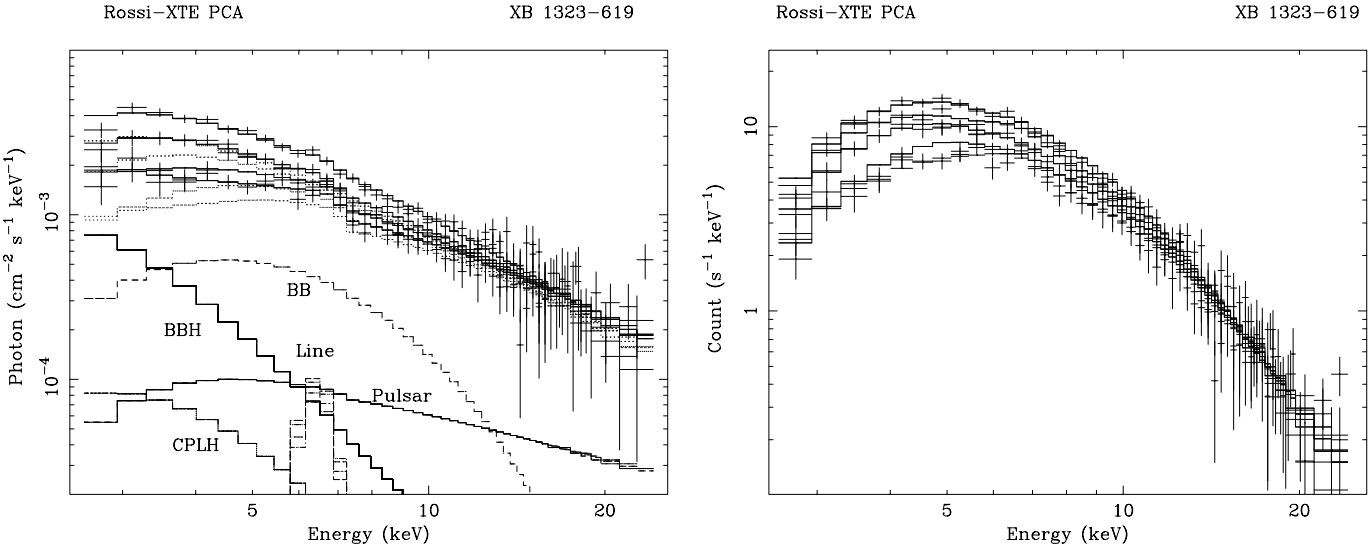

Fig. 5. The four spectra from dip *A* fitted with the best-fit model. Left: unfolded spectrum; right: folded spectrum. The model includes the Comptonized and total model terms *plus* the blackbody (totally absorbed in dipping), the pulsar and line terms as indicated and the cut-off power law halo CPLH and the blackbody halo BBH.

Table 2. Results of fitting non-dip and dip spectra from the first 40 ks of the observations with the model containing continuum terms, an Fe line, the pulsar contribution and the effects of dust scattering both out of, and into, the beam. $N_{\rm H}$ is given in units of 10^{22} atom cm^{-2}.

Spectrum	$N_{\rm H}^{\rm BB}$	$N_{\rm H}^{\rm CPL}$	f	χ^2/d.o.f.
Non-dip	2.7 ± 0.1	2.7 ± 0.1	0	61/51
Shallow	9 ± 1	70 ± 6	0.45 ± 0.01	59/51
Medium	15 ± 2	79 ± 6	0.60 ± 0.02	58/51
Deep	28 ± 4	113 ± 14	0.69 ± 0.02	42/51
Deepest	40 ± 7	179^{+43}_{-30}	0.73 ± 0.02	29/46

and the absorber very blobby so that selection in intensity bands *will* result in mixing data in which $N_{\rm H}$ for the blackbody varies between ∼zero and high values, as the line-of-sight to the point-source passes through the blobby absorber, and so low values of $N_{\rm H}$ will be obtained. Moreover, in our previous analyses of other dipping sources (e.g. XB 1916–053, Church et al. 1997; X 1624–490, Smale et al. 2001), the blackbody has always had a high $N_{\rm H}$ consistent with being covered by the denser central regions of the absorber, whereas the extended Comptonized emisssion has a lower $N_{\rm H}$ as it averages across the absorber.

To investigate these effects, we next analysed the non-dip and 3 dip level spectra selected from the single sub-dip *A*. Results are shown in Table 3 and plotted in Fig. 5 as both unfolded and folded spectra.

These results show that when data is selected more carefully using only a single strong dip, good fits are obtained to all spectra, with substantially improved values of χ^2/d.o.f. The best-fit model consisted of a blackbody with

Table 3. Results of fitting non-dip and dip spectra from dip *A* with the best-fit model. $N_{\rm H}$ is in units of 10^{22} atom cm^{-2}.

Spectrum	$N_{\rm H}^{\rm BB}$	$N_{\rm H}^{\rm CPL}$	f	χ^2/d.o.f.
Non-dip	3.9	3.9	0	42/42
Medium	1.0×10^3	7.7 ± 1.3	0.56 ± 0.20	30/38
Deep	$>4.0 \times 10^4$	20 ± 4	0.70 ± 0.08	37/42
Deepest	$>4.0 \times 10^4$	34 ± 4	0.65 ± 0.04	26/38

$kT = 1.79 \pm 0.21$ keV plus an extended cut-off power law, having power law index $\Gamma = 1.61 \pm 0.04$ keV, with the cut-off energy being fixed at the *BeppoSAX* value of 44 keV. In dipping, the blackbody column density is larger than that of the extended emission component as expected. The results are entirely consistent with the two-component emission model consisting of point-like blackbody emission from the neutron star and extended Comptonized emission from the ADC. The results for the Fe line were also more conclusive in that there was a definite decrease of line intensity in the shallow and medium dip spectra, although, as before, the line became stronger in deep dipping. Thus acceptable fits were obtained by including the line in the same covering factor as for the extended Comptonized emission, as shown in Fig. 5.

4. Discussion

The best-fit model results compare reasonably well with the values obtained from *BeppoSAX* of $kT = 1.77 \pm 0.25$, and $\Gamma = 1.48 \pm 0.01$. The 1–10 keV luminosity of XB 1323−619 was 3.0×10^{36} erg s^{-1} in the *Rossi-XTE* observation, compared with 1.9×10^{36} erg s^{-1} during the *BeppoSAX* observation. The combined effect of the halo

and the X-ray pulsar amounts to ∼8% of the non-dip intensity. Thus, the observed depth of dipping of ∼60% would be increased to ∼70% without these effects, consistent with the maximum covering fraction determined in dipping. Dipping does not however, reach 100% deep, due mostly to the absorber having a blobby structure allowing transmission of radiation between the blobs.

From this observation, we have detected an iron line in XB 1323−619. The energy of the line at 6.43 ± 0.21 keV is interesting because of the question of whether it can originate in the ADC as the evidence indicates. It has been known for some time that iron lines in LMXB tend to have energies of ∼6.6 keV (Asai et al. 2000; White et al. 1985, 1986), suggesting origin in the ADC produced by photoionization followed by recombination. However, Smale et al. (1993) discussed the possible sites of 6.7 keV emission in Cyg X-2 and concluded that the disk was the origin of the emission. In the *ASCA* iron line survey (Asai et al. 2000), the mean energy for 20 sources was 6.56 keV, with only 5 sources having measured energies of 6.5 keV or lower. The mean energy implies a relatively low ionization state as it is equivalent to an ionization parameter ξ of ∼100, where ξ is $L/n\,r^2$. Hirano et al. (1987) had conducted a similar study of iron lines in LMXB using *Tenma* and also carried out simulations of line emission from an ADC of varying ionization state. This showed that iron fluorescence is also possible in the ADC for values of the ionization parameter ∼100. Other authors have measured energies of ∼6.4 keV in particular LMXB sources and have suggested that the line originates in the accretion disk (e.g. Barret et al. 2000). In the dipping, flaring source X 1624–490, we have also detected a broad iron line at 6.4 keV, this agreeing with the energy found by Asai et al. (2000), and investigated the variation of the line in dipping (Smale et al. 2001) and in flaring (Bałucińska-Church et al. 2001). In dipping, the line variation is well-described by giving it the same covering fraction as the extended Comptonized emission of the ADC, strongly suggesting that the line originates in the ADC, even though the energy may be regarded as low for this. In flaring, it was found that the line intensity correlated strongly with the luminosity of the neutron star blackbody emission, providing direct evidence that the line is excited by the central source. Similarly, the 0.65 keV line in XBT 0748–676 (Church et al. 1997), has the same covering fraction as the Comptonized emission. In the present case of XB 1323–619, the line varies in dipping in approximately the same way as the Comptonized emission, except for the apparent presence of the line in deep dipping, which is not understood. It is possible that the measurement is complicated by the fragmented nature of the absorber. Further work will be necessary to clarify the line behaviour in dipping and we will investigate this in more detail using the observation of XB 1323−619 with *XMM* that is scheduled. Thus the evidence supports origin of the line in the ADC as in other LMXB, although its energy implies it is fluorescent. Many workers argue that it is not possible to have a low ionization state in the ADC since the electron temperature can be high ($kT_e \gtrsim 15$ keV in this source; Sect. 1). However, the *ASCA* LMXB line survey shows that the ionization state *is* relatively low, since the mean energy of 6.56 keV corresponds to $\xi \sim 100$ (Dotani, priv. comm.) so that there is a discrepancy between observation and simple theoretical expectations.

We also comment on the lack of detection of a reflection component in the present data. In fact, there has been a general lack of detections of reflection components in LMXB, and reported detections in a very small number of sources have been ambiguous. In *Ginga* work on LMXB, a broad edge-like structure above ∼7 keV in XB 1608–522 was fitted either by partial absorption or a reflection component (Yoshida et al. 1993). The *ASCA* survey of LMXB (Church & Bałucińska-Church 2001) failed to detect reflection in any of the sources investigated. We can argue (see also Bałucińska-Church et al. 2001) that this may be due to the large size of the ADC, discussed below, typically having radius ∼50 000 km. One consequence of this is that the accretion disk will be shielded from exposure to the neutron star source by the hot reflector of the ADC preventing reflection in the disk. Illumination of the disk by the ADC will not produce an observable reflection component given the large optical depth of the corona (Church 2001). In black hole binaries, e.g. in Cyg X-1, the ADC appears to be much less extended (Church 2001) so reflection may take place.

Spectral fitting shows that the Comptonizing ADC region is clearly extended as it can only be modelled by a progressive covering fraction, as we have found in the other dipping sources, e.g. XB 1916–053 (Church et al. 1997) and X 1624–490 (Smale et al. 2001). This is reinforced by measurements of ADC radius based on dip ingress time determination in several dipping sources (Church 2001) showing that $r_{\rm ADC}$ is typically 50 000 km or 15% of the radius of the accretion disk. In XB 1323−619, $r_{\rm ADC}$ is 22 000–54 000 km (reflecting the uncertainty in ingress time). The smallest value obtained so far is in XBT 0748–676 where we obtain $r_{\rm ADC} = 8500 \pm 3000$ km from the dip ingress time, and 3500 ± 1500 km from the eclipse ingress time, consistent within the errors. The largest value is 53 000 km in the bright source X 1624–490 (Church 2001), approximately half the radius of the accretion disk. Thus, in all sources the ADC radius is many times larger than the neutron star radius. In the case of XBT 0748–676, Bonnet-Bidaud et al. (2001) obtained $r_{\rm ADC} \approx 2000$ km from the *XMM* observation. However, the light curve of this observation was interpreted by them as flaring separated by low intensity intervals, whereas the *ASCA* light curve (Church et al. 1998a) with a similar shape was proven by spectral analysis to represent several intervals of dipping per orbital cycle. Thus the "flaring" actually consisted of a temporary return from dipping to the non-dip state. This may have led to the somewhat smaller value of $r_{\rm ADC}$ deduced. Apart from the very large radius, it can also be argued that the ADC is *thin* (Smale et al. 2001). The extended size has several significant consequences as indicated in Sect. 1. Firstly, it does not allow models in

which Comptonization is localized to the neighbourhood of the neutron star. Secondly, it is not expected that disk blackbody emission will be observed since the ADC (of high optical depth; Church 2001) covers all of the X-ray emitting disk so that all disk blackbody radiation will be Comptonized, explaining naturally the dominance of Comptonization in LMXB. The expectation that disk blackbody will not be observed agrees with the results of Church & Bałucińska-Church (2001) from a survey of LMXB with *ASCA* and *BeppoSAX* who found that in the majority of cases, the inner disk radius was substantially smaller than 10 km, the neutron star radius.

The large size of the ADC has implications for different representations of Comptonization. There has been an increasing use in recent years (Guainazzi et al. 1998; Oosterbroek et al. 2001) in analysis of *BeppoSAX* data of the model DISKBB + COMPTT i.e. disk blackbody plus Comptonization described by the COMPTT model in *XSPEC* based on the prescription of Titarchuk (1994). It is sometimes claimed that COMPTT is a better representation of Comptonization at low energies than a cut-off power law, which could be inaccurate because of a lack of seed photons below 1 keV However, a major consequence of an ADC radius of 50 000 km is that the spectrum of the accretion disk *under the ADC* is very soft. Calculation of this spectrum using the temperature profile $T(r)$ from thin disk theory shows that the spectrum peaks between 0.001 and 0.1 keV for source luminosities between 10^{36} and 10^{38} erg s^{-1}, providing a huge sea of very soft photons. Thus, the cut-off power law is perfectly applicable.

Moreover, in applications of the COMPTT model, it is often the case that the temperature of the seed photons is allowed to become large, i.e. ∼1 keV (e.g. Guainazzi et al. 1998). In the model, the seed photons are described by the Wien approximation, i.e assuming that the temperature of the seed photons $kT_{\rm w}$ is much less than the X-ray energies in the spectrum: $kT_{\rm w} \ll h\nu$. For values of $kT_{\rm w}$ ∼1 keV derived from spectral fitting, this condition is only satisfied above ∼5 keV so that use of this model leads to a substantial underestimation of the spectrum at energies below this.

Finally, it should be pointed out that these arguments based on the large size of the ADC provide a justification for the two-component model used here, and found to fit the spectra of many LMXB. The model consisting of point-source blackbody emission from the neutron star plus Comptonized emission from an extended ADC, seeded by the soft photons from the disk vertically beneath the ADC, has implications which are entirely consistent with observation. For example, if the ADC is large and of high optical depth, it is not expected that diskblackbody radiation will be observed, consistent with the *ASCA* survey results. On the other hand, all accretion disk theory requires a substantial fraction of the total emission to be from the neutron star. Modelling of neutron star atmospheres (Madej 1991) shows that electron scattering does not greatly modify the blackbody spectrum. Thus, blackbody emission from the neutron star *should* be seen, and applying the two-component model to many LMXB reveals that a blackbody component completely consistent with origin on the neutron star is always present in varying degrees.

Acknowledgements. R. B. was funded by PPARC Grant 1997/S/S/02401.

References

Angelini, L., Church, M. J., Parmar, A. N., Bałucińska-Church, M., & Mineo, T. 1998, A&A, 339, L41
Asai, K., Dotani, T., Nagase, F., & Mitsuda, K. 2000, ApJS, 313, 571
Bałucińska-Church, M., Church, M. J., Oosterbroek, T., et al. 1999, A&A, 349, 495
Bałucińska-Church, M., Humphrey, P. J., Church, M. J., & Parmar, A. N. 2000, A&A, 360, 583
Bałucińska-Church, M., Barnard, R., Church, M. J., & Smale, A. P. 2001, A&A, 378, 847
Boella, G., Chiappetti, L., Conti, G., et al. 1997, A&AS, 122, 327
Bonnet-Bidaud, J. M., Haberl, F., Ferrando, P., Bennie, P. J., & Kendziorra, E. 2001, A&A, 365, 282
Bradt, H. V., Rothschild, R. E., & Swank, J. H. 1993, A&AS, 97, 355
Church, M. J. 2001, Proc. 33rd Scientific Assembly of COSPAR, Warsaw, July 2000, Adv. Space Res., in press
Church, M. J., & Bałucińska-Church, M. 2001, A&A, 369, 915
Church, M. J., Inogamov, N. A., & Bałucińska-Church, M. 2001, A&A, submitted
Church, M. J., Dotani, T., Bałucińska-Church, M., et al. 1997, ApJ, 491, 388
Church, M. J., Bałucińska-Church, M., Dotani, T., & Asai, K. 1998a, ApJ, 504, 516
Church, M. J., Parmar, A. N., Bałucińska-Church, M., et al. 1998b, A&A, 338, 556
Courvoisier, T. J.-L., Parmar, A. N., Peacock, A., & Pakull, M. 1986, ApJ, 309, 265
Forman, W., Jones, C., Cominsky, L., et al. 1978, ApJS, 38, 357
Gottwald, M., Parmar, A. N., Reynolds, A. P., et al. 1995, A&AS, 109, 9
Guainazzi, M., Parmar, A. N., Segreto, A., et al. 1998, A&A, 339, 802
Hirano, T., Hayakawa, S., Nagase, F., Masai, K., & Mitsuda, K. 1987, PASJ, 39, 619
Jahoda, K., Swank, J. H., Giles, A. B., et al. 1996, in EUV, X-ray and Gamma-ray Instrumentation for Astronomy VII, ed. O.H. Siegmund (Bellingham, WA), 59
Jonker, P. G., van der Klis, M., & Wijnands, R. 1999, ApJ, 511, L41
Martin, P. G. 1970, MNRAS, 149, 221
Mathis, J. S., & Lee, C.-W. 1991, ApJ, 376, 490
Mauche, C. W., & Gorenstein, P. 1986, ApJ, 302, 371
Mitsuda, K., Inoue, H., Nakamura, N., & Tanaka, Y. 1989, PASJ, 41, 97
Oosterbroek, T., Parmar, A. N., Sidoli, L., in't Zand, J. J. M., & Heise, J. 2001, A&A, 376, 532
Parmar, A. N., White, N. E., Giommi, P., & Gottwald, M. 1986, ApJ, 308, 199

Parmar, A. N., Gottwald, M., van der Klis, M., & van Paradijs, J. 1989, ApJ, 338, 1024
Predehl, P., & Klose, S. 1996, A&A, 306, 283
Predehl, P., & Schmitt, J. H. M. M. 1995, A&A, 293, 889
Smale, A. P., Mason, K. O., White, N. E., & Gottwald, M. 1988, MNRAS, 232, 647
Smale, A. P., Mukai, K., Williams, O. R., Jones, M. H., & Corbet, R. H. D. 1992, ApJ, 400, 330
Smale, A. P., Done, C., Mushotzky, R. F., et al. 1993, ApJ, 410, 796
Smale, A. P., Church, M. J., & Bałucińska-Church, M. 2001, ApJ, in press
Titarchuk, L. 1994, ApJ, 434, 313
Van der Klis, M., Jansen, F., van Paradijs, J., & Stollman, G. 1985, Space Sci. Rev., 30, 512
Warwick, R. S., Marshall, N., Fraser, G. W., et al. 1981, MNRAS, 197, 865
White, N. E., & Swank, J. H. 1982, ApJ, 253, L61
White, N. E., Peacock, A., & Taylor, B. G. 1985, ApJ, 296, 475
White, N. E., Peacock, A., Hasinger, G., et al. 1986, MNRAS, 218, 129
Yoshida, K., Inoue, H., Mitsuda, K., Dotani, T., & Makino, F. 1995, PASJ, 47, 141
Yoshida, K., Mitsuda, K., Ebisawa, K., et al. 1993, PASJ, 45, 605